CEAS Space Journal
https://doi.org/10.1007/s12567-025-00613-y

ORIGINAL PAPER

Mathematical analysis approach for the pre-design of landing platforms with alignment, levelling, and lowering function

Jan Bertram[1] · **Lars Witte**[1]

Received: 17 September 2024 / Revised: 3 March 2025 / Accepted: 1 April 2025

Abstract
The objectives for celestial body exploration especially regarding lunar exploration became more and more demanding over recent years. New landers are needed for missions in the Artemis programme by the National Aeronautics and Space Administration (NASA) or the Terra Novae exploration programme by the European Space Agency (ESA) that offer a great deal of reliability and versatility. A system that can level, align, and lower the whole landing platform could offer a lot of benefits in comparison to older lander concepts without such a system. Challenges like unevenness of the ground, slopes in the area of the landing site, as well as different compression of the lander legs can be counteracted. Additionally, access to the lander's payload bay is simplified by lowering the landing platform as a whole closer to the ground. This study takes a closer look at an approach for the conceptual design of such a mechanism in the early design stages of a lander using a minimal number of known parameters and low computational expenditure. The approach of calculating the motion of the lander and the forces due to the motion on each of the legs primary strut interfaces is first explained and then demonstrated for the European Large Logistics Lander (EL3) on the basis of a mechanism, which moves the primary interface of each landing leg in the vertical axis of the lander.

Keywords Lunar exploration · Alignment and levelling kinematic · Planetary lander · Landing platform

1 Introduction

In recent years, interest in lunar exploration through programs like NASA's Artemis programme or the Terra Novae exploration programme (formerly European Exploration Envelope Program or E3P) of the ESA has increased again [1–4]. Additionally, the advance of science goals to target more difficult landing sites e.g. near the poles [5] lead to a need for new, improved, and more flexible landing platforms that can meet the requirements of a range of different payloads and landing sites [6, 7].

The state-of-the-art landing platforms use dampened legs to compensate for landing shock that happens at touchdown. After touchdown, however, they are not able to compensate for the incline due to uneven ground surface or different amounts of crushing of the damping elements. This leads to a tilted landing platform in almost every case. Proposals for actively controlled damping systems [8–10] and in-situ change of landing leg geometry [11, 12] for inclined landing sites exist. The systems that can compensate for the decrease in leg length due to crushing of the damping elements are being actively studied as well [13]. None of them, however, try to fully compensate the tilt of the landing platform after touchdown or lower it to the ground for easy access to the lander.

A non-levelled or -lowered platform already lead to challenges in the past. Most notably are examples like the NASA Apollo missions where astronauts had to offload equipment from the Lunar Module (LM) using a small integrated crane [14] (Fig. 1), or the Helmholtz Association of German Research Centres ROBEX mission, which utilised an autonomous robot capable of extracting instruments from the lander using a robotic arm [15] (Fig. 2). Lowering the platform for operations of this kind has the potential to make them a lot easier than in the past. Another example is NASA's Apollo 15 mission, in which the LM was located partially inside a small crater after touchdown, leading to a

✉ Jan Bertram
jan.bertram@dlr.de

Lars Witte
lars.witte@dlr.de

[1] German Aerospace Center (DLR), Institute of Space Systems, Bremen, Germany

Published online: 23 April 2025

Fig. 1 Apollo 12 astronaut Alan Bean offloading equipment from the Lunar Module's Scientific Equipment Bay (image credit: NASA, AS12-46-6783 [14])

tilt angle of approximately 11° from the horizontal [16]. The maximum tilt angle for safe lunar lift-off is not stated in [16] and is hard to place exactly. The Apollo Lunar Module Landing Strategy [17] states a maximum tip over balance point of approximately 40° but does not mention take-off. Baker placed the maximum vehicle inclination for take-off at 15° [18] but without explaining the origin of this value. In any case the limit for a safe departure is increased and possible problems avoided by implementing a levelling kinematic.

Based on the previous examples, reducing or fully negating the tilt angle, as well as lowering the landing platform, would enable more use cases for these landers and extend already existing ones. From mounting tilt sensitive instruments and ascent stages, simplifying cargo logistics, to opening up new landing sites that were deemed unfeasible in past missions, an alignment and levelling kinematic is able to drastically improve the landers capabilities. Interference with the damping characteristics of the legs themselves has to be ruled out. This publication addresses one possible mechanism, which linearly moves the interface (I/F) of the primary strut of each landing leg up or down the side of the lander's body, thereby changes its geometry and aligning, levelling, and lowering the landing platform in the process.

The first design of such a kinematic usually requires complex calculations as a landing platform may be compared to a parallel manipulator like a hexapod (also known as a Gough–Stewart platform). The positioning of a platform like this is normally done using inverse kinematics in which the actuator (here: the landing legs) parameters are calculated based on the desired position of the end-effector (here: the landing platform). Some problems regarding inverse kinematics can be solved analytically but, in most cases, numerical approaches using high degree polynomials have to be implemented. This can make comparisons between different design ideas tedious and time consuming [19, 20]. Additionally, challenges like singularity constraints, non-linear behaviour, and secondary unwanted motions of parts that happen due to primary wanted motions (so-called parasitic motion) are introduced to the system, all of which increase the difficulty of the computation further [21, 22]. Even though a final design definitely needs to consider all these effects, a first approximation allows to get usable results quickly and to discern whether a design is viable or not.

The viability of a design is, however, not only limited by the geometric constraints of the system but also by the forces acting on it. Therefore, forces acting on the actuators have to be considered. In early design stages, there is inherently only preliminary knowledge of the entire geometry of the system to conduct a finite element analysis (FEA) in a suited computer program. This includes e.g., exact dimensions, material choice, mass distribution, and the structural design of the lander body. More importantly, using FEA programs also includes model generation, meshing, material assignment, etc. and this effort is not always justifiable these early design phases, especially when multiple different designs have to

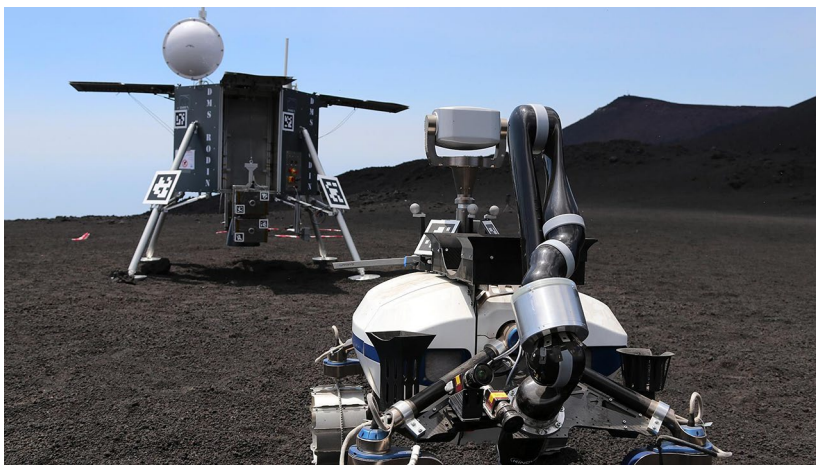

Fig. 2 Rover LRU-2 (Light Weight Rover Unit) during a demo mission on Mount Etna

be evaluated quickly. On the other hand, simple analytical approaches like a calculation using a statically determined system with simply supported legs fail if the lander has four or more legs as this leads to an overdetermined system. The simplifications in which two legs of a four-legged lander are loaded with the same force are possible to be calculated as a determined system, but for more than four legs this approach does not work.

The proposed approach to overcome the disadvantages of either an overly simplistic or too high-fidelity model is to generate a basic truss structure as an analogue of the landing system and calculate the forces acting in each beam and on the nodes of the truss using the direct stiffness method (DSM). The DSM is the basis of many FEA programs, but when programmed directly circumvents the need to write code to interface with an existing FEA program. Additionally, it is based on matrices, which can easily be solved by a computer [23–25]. Further, it is parametrised, and therefore, possible to be automated. Thereby allowing for "what-if"-studies comparing slight design variations to one another quickly and early in the design process.

The subsequent chapters explore an efficient approach for both geometric and load computation for a first design of an alignment, levelling, and lowering kinematic that allows a quick comparison between different lander configurations, sizes, payloads, and masses.

2 Mathematical approach

Analytical approaches often fall short of being able to solve the complex non-linear differential equation needed to fully describe a parallel manipulator. A numerical approach has to be utilised in most cases, as well as for this publication.

The computations for this publication are carried out using MATLAB Version R2019a and R2023b, naturally other software could also be used. A validation of the computed force results was conducted using MSC Patran 2018 as pre-/post-processor with MSC Nastran (SOL101) as solver. Additional information on the validation can be found in Sect. 2.8 Validation of force computation.

2.1 Geometric definitions and coordinate systems

In a first step, the geometric definition of the lander has to be simplified into a generic model. This allows for a simple adaptation of the lander type and its dimensions to compare different designs.

A lander generally consists of three or more legs, which are made up of a primary and two secondary struts. In most designs, the primary strut takes most of the load during touchdown and while standing on the ground, while the secondary struts stabilise the primary strut. In general, a distinction is made between two different landing leg configurations [26, 27]:

1. Cantilever: secondary struts are attached to the immovable part of the primary strut.
2. Inverted tripod: secondary struts are attached to the movable part of the primary strut closer to the footpad.

This differentiation is important for overall lander characteristics like stability, mass, and landing dynamics. Since the legs are assumed to be rigid after the initial touchdown, this differentiation is of less importance here and will, therefore, not be explained further, however, both configurations can be calculated with this approach.

The most important dimensions of a given lander are depicted in Fig. 3. These are the overall dimensions of the lander's body (height h_L and width of the body d_L) and its landing legs (length of primary strut L_{S1} and its upper $L_{S1,upp}$ and lower segment $L_{S1,low}$, and the length of the secondary struts L_{S2} and L_{S3}), as well as the location of the centre of gravity (CoG) inside the body (height of CoG h_{CoG}). In an actual lander, each leg has different dimensions due to the difference in crushing of the honeycomb dampeners during touchdown. This affects the location of the CoG slightly, as the lander loses its rotational symmetry, meaning it cannot be solely described by a height anymore. A further examination of this effect is neglected here, however, the difference in leg dimensions are considered for the calculations. Figure 3 also indicated the names of the I/Fs for each strut used, which are numbered like the struts themselves (the primary strut S1 connects to I/F1 and so on). The connection between a primary strut and the two connecting secondary struts is denoted as I/F4.

For the description of the lander in three-dimensional space, two different coordinate systems are being utilised. A body coordinate system and a global coordinate system.

The right-handed body coordinate system is used to describe the I/F positions of the leg's primary and secondary strut to the landing platform and forces or movement relative to the landing platform. Its origin is located at the central point of the lower side of the lander body. The x-axis x_{body} points in a radial direction towards I/F1 of leg 1. The z-axis z_{body} is normal to the x-axis and pointed upwards towards the upper side of the lander body. The y-axis y_{body} completes the right-handed coordinate system and points towards leg 2.

For simplicity of transformation between the two coordinate systems, the origin of the global coordinate system is kept at the same point and does not move during alignment and lowering. Its z-axis z_{glob} points upwards against the direction of the local gravitational vector. This coordinate system is mainly used to describe global motion of the lander during alignment and levelling. Both coordinate

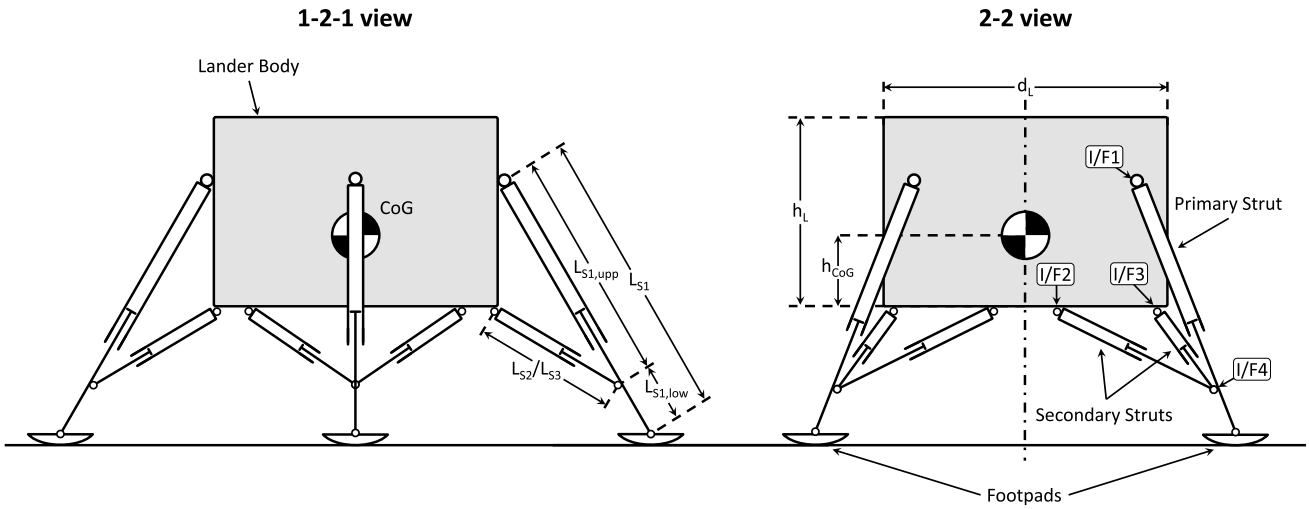

Fig. 3 Most important dimensions of a generic (inverted tripod) lander (adapted from [26])

systems are depicted along with the global pitch (θ) and roll (ϕ) angles in Fig. 4.

The transformation from one coordinate system to the other is done using Euler angles, more specifically Tait–Bryan angles. Here, the angles about x, y, and z are γ, β, and α, respectively. It is important to keep one sequence in which the rotations around the axes is computed, as changing the order of the rotations leads to different results for the same angles. The most common order of rotations used in the spaceflight regime is x-y-z (extrinsic rotations) or z-y'-x'' (intrinsic rotations), both of which are interchangeable. To get the angles α, β, and γ the global pitch (θ) and roll (ϕ) angle are first transformed into the axis-angle representation. In this representation, a rotation of a vector is simply defined as a rotation by a specific amount θ_e around a unit vector $\vec{e}$. In this case, the axis around which the coordinates have to be rotated is a line orthogonal to the vertical axes of the two coordinate systems between which the coordinate transformation shall take place. It is computed by forming the dot product of unit vectors in the two vertical axes. For example, the axis around which a rotation between the global and the body coordinate system is conducted, can be computed using:

$$\vec{e} = \overrightarrow{z_{glob}} \cdot \overrightarrow{z_{body}} \tag{1}$$

The angle θ_e is simply the angle between the two vectors $\overrightarrow{z_{glob}}$ and $\overrightarrow{z_{body}}$.

$$\cos\theta_e = \frac{\overrightarrow{z_{glob}} \cdot \overrightarrow{z_{body}}}{\left|\overrightarrow{z_{glob}}\right|\left|\overrightarrow{z_{body}}\right|} \tag{2}$$

The Euler angles α (yaw), β (pitch), and γ (roll) are computed in the next step.

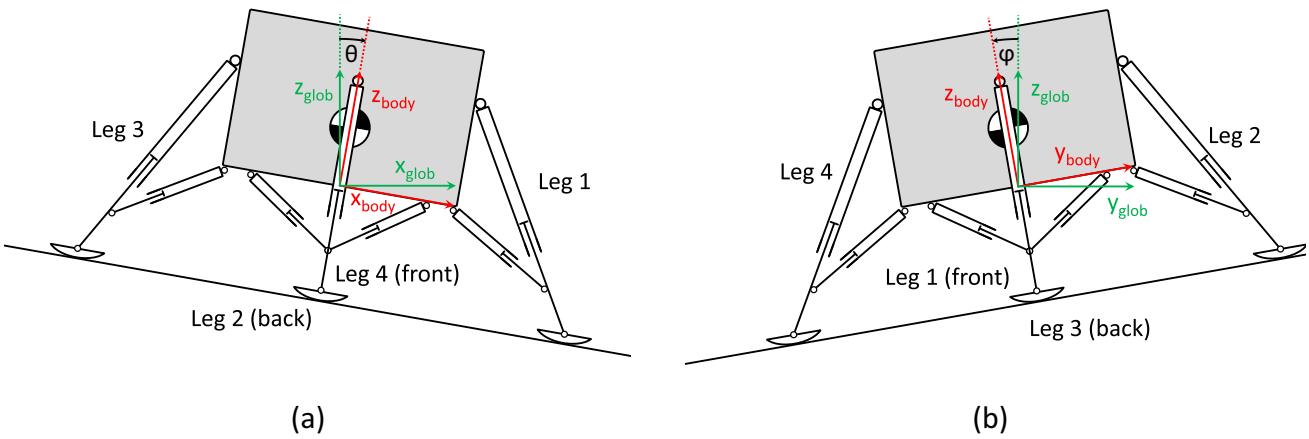

Fig. 4 Coordinate system: (a) Lander on a 10° slope (tilted around the y-axis); (b) Lander on a 10° slope (tilted around the x-axis)

$$\alpha = \arctan\left(\frac{e_x \cdot e_y \cdot \left(1-\cos\theta_e\right) + e_z \cdot \sin\theta_e}{1-\left(e_y^2+e_z^2\right)\cdot\left(1-\cos\theta_e\right)}\right) \tag{3}$$

$$\beta = \arcsin\left(-\left(e_x \cdot e_z \cdot \left(1-\cos\theta_e\right) - e_y \cdot \sin\theta_e\right)\right) \tag{4}$$

$$\gamma = \arctan\left(\frac{e_y \cdot e_z \cdot \left(1-\cos\theta_e\right) + e_x \cdot \sin\theta_e}{1-\left(e_x^2+e_y^2\right)\cdot\left(1-\cos\theta_e\right)}\right) \tag{5}$$

After calculating these Euler angles, the transformation matrix R is defined in the usual way and the transformation is done by pre-multiplying with the vector that shall be transformed.

$$R = R_z(\alpha)R_y(\beta)R_x(\gamma) \tag{6}$$

$$= \begin{bmatrix} \cos\alpha\cos\beta & \cos\alpha\sin\beta\sin\gamma - \sin\alpha\cos\gamma & \cos\alpha\sin\beta\cos\gamma + \sin\alpha\sin\gamma \\ \sin\alpha\cos\beta & \sin\alpha\sin\beta\sin\gamma + \cos\alpha\cos\gamma & \sin\alpha\sin\beta\cos\gamma - \cos\alpha\sin\gamma \\ -\sin\beta & \cos\beta\sin\gamma & \cos\beta\cos\gamma \end{bmatrix}$$

2.2 Simplifications and assumptions for lander geometry, motion, and forces

While some properties of the lander like its geometry and orientation are known by definition or measurement, a few assumptions have to be made for other characteristics. This is necessary to make the script easily adaptable while still keeping it in a feasible operational framework without too many redundant code pieces.

2.3 Definitions and known parameters

D1. The orientation of the lander after touchdown is known in the form of roll around the x_{glob} and pitch around y_{glob}.
D2. The lengths of all landing leg struts (primary and secondary), after landing and crushing of the dampening elements, are known and these lengths do not change during alignment and levelling.
D3. The position of all primary and secondary strut interfaces (I/F1 to I/F3) relative to the body coordinate system are known based on the lander design.

2.4 Assumptions

A1. The positions of the primary strut interfaces only change in the direction of z_{body}.
A2. The position of the secondary strut interfaces does not change relative to the body coordinate system as they are assumed not to be actuated.
A3. As a first approximation, the ground is assumed to be locally described by a plane without any bumps or changes in inclination.
A4. The motion of the platform is assumed to happen slowly, i.e. inertial effects can be neglected and all forces are assumed to be quasi-static.
A5. The platform is assumed to be sufficiently described with three degrees of freedom (DoF):

- Translational movement along z_{glob}
- Rotational movement around x_{glob} (roll)
- Rotational movement around y_{glob} (pitch)
- Other translational movement, yaw around z_{glob}, and parasitic motion, is neglected.

This calculation, based on alignment and height above ground, is meant to provide a baseline for comparison of different lander geometries in an early design stage. A first design of the alignment and levelling kinematic may be derived from its results. The length needed for the linear drive of the primary strut interface to the lander and the loads on the legs and the forces needed to drive the lander from its landing position into the final desired position can be estimated. These insights can then be used to aid in support for early design decisions. For a full system design at a later point in time, more advanced dynamic simulations might be needed.

2.5 Calculation of lander motion

The numerical approach chosen for the calculation combines vector calculus and trigonometry as well as non-linear numerical optimisation to calculate the interface positions of each leg for the desired height and alignment of the landing platform.

In a first step, the location and orientation of the ground plane in the global coordinate system is calculated. The ground plane is not assumed to be known but is rather calculated based on the coordinates of the lander's footpads, all of which have contact with the ground. As a result, the ground plane parameters are calculated from the known lander position and the length of its landing leg struts after touchdown. The calculation is, therefore, only based on the parameters of the lander and not on external factors, i.e. an internal

measurement of the state of the lander is enough to calculate a path to alignment and levelling of the landing platform.

Based on the known coordinates of the I/Fs one to three and the lengths of each leg part (see defined parameters D2 and D3), it is possible to calculate the coordinates of I/F4. For each combination of strut lengths and I/F locations, only two locations are conceivable for I/F4, one of which would locate the landing leg inside the lander body, i.e. it can be ruled out. While it is possible to analytically calculate the exact position of a third point based on the known coordinates of two others in a two-dimensional case, it is more complex in a three-dimensional case. In theory, considering the coordinates of the I/Fs as the centre of spheres with a radius r (which is set to the known distance from I/F4 to the respective I/F on the lander body), the point where all three spheres meet should be the location of I/F4. Due to measurement inaccuracies, however, any difference between the measured and the actual length value of the struts may lead to an overdetermined or underdetermined system. In these cases, more than one or no solution exist, hence an analytical calculation is not possible. The same problem is faced in geo-positioning, i.e. a similar approach can be utilised in the triangulation of the location of I/F4. Inaccuracies in the measurement are counteracted by searching for a local optimum of a cost function f_{cost} (see Eq. (7)), which uses a first guess of the coordinates of I/F4, denoted as point P_4, as an input. From here an iterative calculation is used to find this optimum. The coordinates of I/F1 to IF/3 are denoted as P_1 to P_3, with their distances to P_4 denoted as r_1 to r_3, respectively.

$$f_{\text{cost}}(P) = \sum_{i=1}^{n} \begin{pmatrix} \left(\left| \overrightarrow{P_1 P_4} \right| - r_1 \right)^2 \\ \left(\left| \overrightarrow{P_2 P_4} \right| - r_2 \right)^2 \\ \left(\left| \overrightarrow{P_3 P_4} \right| - r_3 \right)^2 \end{pmatrix} \tag{7}$$

The cost function serves as a geometrical constraint function making sure only geometrically possible solutions are found. To increase the accuracy, the difference between the distance of the guessed position P_4 to the interfaces and the actual distances r is squared before the sum is calculated. By iteratively varying the guess of P_4, a local minimum for f_{cost} can be found. This calculation is done for each leg individually. In MATLAB, the fminsearch-function (a multidimensional unconstrained non-linear minimisation) is utilised, which uses the so called "Nelder-Mead method" to minimise the cost function. From the now known coordinates of I/F1 and I/F4, the coordinates of the footpads, which lay on the ground plane, are calculated using vector calculus. The ground plane can be described based on this, e.g. in form of the Hesse normal form.

After the ground plane is known, the lander body is tilted and lowered or raised slightly in the global coordinate system from its first orientation after touchdown towards a specified aligned and levelled orientation. The footpads will no longer mathematically lay on the ground plane after this operation, i.e. the geometry of the lander has to be adapted. There is a multitude of different possible approaches to accomplish this: e.g. linear movement of the primary strut interface using a linear actuator, movement of the I/F of the primary strut on an arc by attaching it to an additional rod that can be rotated away from the lander body, changing the lengths of the struts using an internal screw mechanism etc. In this publication, an approach of linearly moving the I/F of the primary strut up and down (in direction of $z_{\text{body}} \rightarrow$ see also assumed parameter A1) is chosen as it is easily implementable into existing lander designs without tampering with the internal mechanics of the landing legs and is adaptable for a multitude of lander sizes and masses. By adapting the coordinates of I/F1 of each leg in the direction of z_{body} so that the footpads lie on the ground plane again (within a small error margin of 0.1 mm), the travel distance of the I/Fs can be calculated. By slowly approaching the desired final orientation and height above ground of the lander body in a step-wise manner, a discrete motion path for each I/F results. The accuracy increases with the number of in-between steps. Figure 5 shows an exemplary lander transitioning from an initial touchdown orientation in State 0 (which is tilted by 15°) to a final aligned and levelled orientation in State 5 with four in-between steps. The lander is also lowered closer to the ground during the entire operation. This becomes apparent when comparing State 0 to State 5 in which the lander body's lowest point comes to rest approximately one metre below its initial position in State 0.

2.6 Force calculation

For purpose of the proposed method, the lander is described for each discrete state as a truss structure with simply supported feet due to friction between the footpads and the ground and a force acting in the CoG. As such, the calculation can be simplified and automated for all landers. This makes usage of high-fidelity, but potentially resources-intensive simulation tools such as FEA obsolete for an initial dimensioning, reduces the time needed to compare different possible designs, and therefore, increases efficiency. This is especially true for possible automated "what-if"-studies, comparing a multitude of slight variations for the optimal design. The calculation method used here is the so-called direct stiffness method (DSM), which is the basis for most modern FEA or FEM applications. A matrix-based approach is used which is fast and uses less memory than other methods to calculate the forces acting inside a truss-like structure. By coupling nodes and their translation due to external

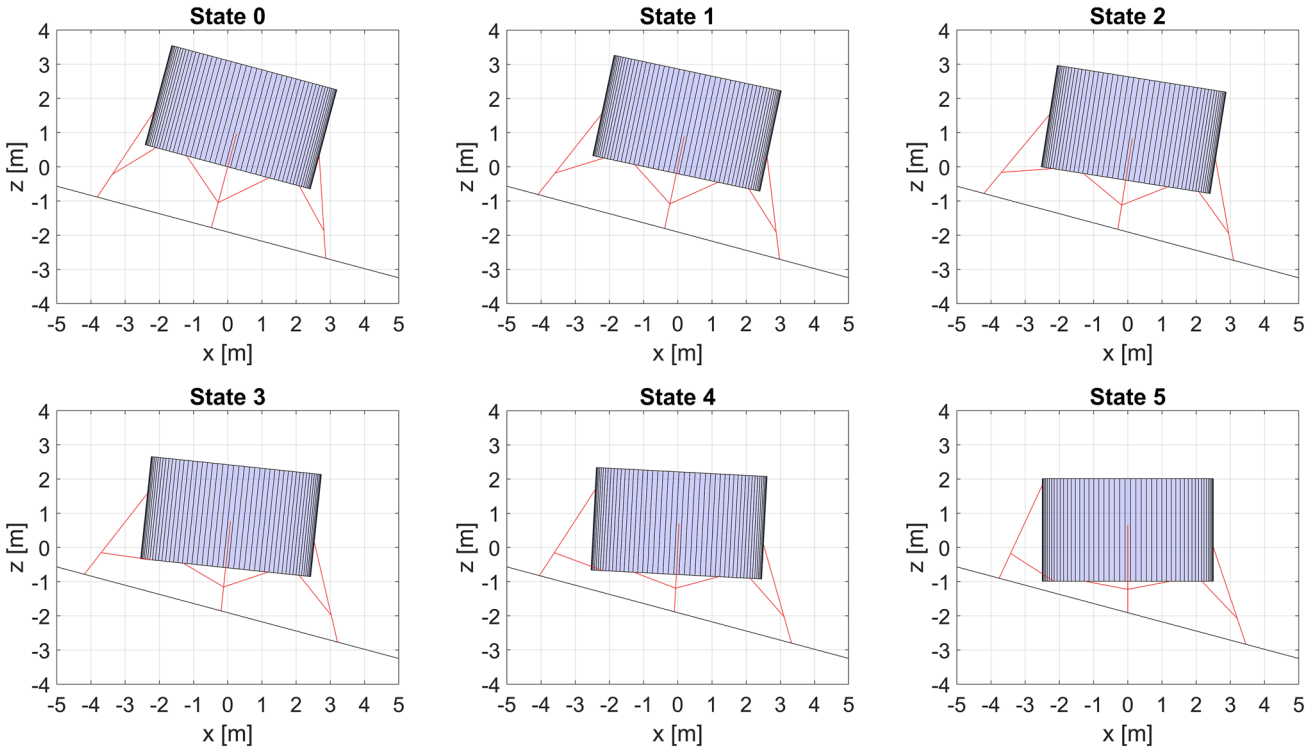

Fig. 5 Transition of lander from landing position to aligned, levelled, and lowered position: example of motion of the lander on a ground slope of 15° from State 0 (right after landing) to the final state (here: State 5) in which the lander is aligned, levelled, and lowered

forces using a stiffness matrix, acting forces in the system are calculated [23–25, 28].

It would also be possible to use any FEM program to do a FEA and calculate the reaction forces this way. However, transferring the coordinates to a FEM-program, creating the mesh, applying the correct material properties and so forth, requires a translation program which transfers the input values (i.e. dimensions of the lander, etc.) into ones that are logical to the FEM-program. By using the DSM these steps can be circumvented. This not only allows the user to do all calculations in one place without switching programs, but also increases efficiency as it reduces time needed to compare very different designs to one another.

It works for landers with as many or as few legs as needed, is automatable, and allows for easy adaptation of the system's properties. Further, it is very accurate for small displacements (accuracy has been validated in this publication to less than 1% difference to results from an FEA program; cf. Table 1), offers the ability to individually change the mechanical properties and boundary conditions of each of the struts easily, and includes bending effects of the struts. Doing this also allows to include effects like the mechanical compliance of the dampening elements in the struts and of the interaction between the footpads and the lunar regolith in a simplified variant if needed. All of this, combined with the simplicity and easy parametrisation of the DSM allows for easy "what if"-studies. This allows the comparison of slight design differences to quickly improve a landers design in early development phases.

To implement the DSM, the system has to be simplified into a truss structure consisting of nodes and connecting beams. An example of a simplified lander system with all of the struts is depicted in a trimetric representation in Fig. 6. Here, the struts that actually exist, i.e. the legs of the system, are depicted in different shades of red. The struts depicted in shades of grey are connecting the legs to one another. They act as mechanical support to the legs, which in reality would be provided by the structure of the lander body. Differently shaded/saturated colours are used to indicate three-dimensional placement in the two-dimensional figure. Each leg of the lander has a total of four red leg struts (split at each I/F) and six struts connecting the I/Fs at the lander body with each other and the CoG. Additionally, one strut is used to connect the secondary strut I/Fs of one leg with the ones next to it. All connection points are realised as joints with movement allowed in every direction except for the two beams making up the primary strut. These do not allow rotation relative to one another. The connection to the ground is realised as simply supported beam elements for each discrete, quasi-static calculation step.

Table 1 Comparison of force results from DSM and FEA analysis on the footpads in the inertial body coordinate system for a ground slope of 15° in the direction of leg 1

0° roll/15° pitch		Leg 1	Leg 2	Leg 3	Leg 4
x_{body}	DSM	– 1225.7 N	– 459.7 N	42.0 N	– 459.5 N
	Patran/Nastran (SOL101)	– 1227.6 N	– 449.9 N	24.6 N	– 449.9 N
	Absolute difference	1.9 N	– 9.8 N	17.4 N	– 9.6 N
	Relative difference	0.16%	– 2.13%	41.43%	– 2.09%
y_{body}	DSM	– 0.3 N	– 633.7 N	0.0 N	633.9 N
	Patran/Nastran (SOL101)	0.0 N	– 626.1 N	0.0 N	626.1 N
	Absolute difference	– 0.3 N	– 7.6 N	0.0 N	7.8 N
	Relative difference	N/A	– 1.20%	0.00%	1.23%
z_{body}	DSM	3130.0 N	1961.8 N	794.1 N	1962.2 N
	Patran/Nastran (SOL101)	3129.9 N	1962.0 N	794.2 N	1962.0 N
	Absolute difference	0.1 N	– 0.2 N	– 0.1 N	0.2 N
	Relative difference	< 0.01%	– 0.01%	– 0.01%	0.01%
Absolute axial compression	DSM	3361.4 N	2112.2 N	795.2 N	2112.6 N
	Patran/Nastran (SOL101)	3362.0 N	2108.0 N	794.6 N	2108.0 N
	Absolute difference	– 0.6 N	4.2 N	0.6 N	4.6 N
	Relative difference	– 0.02%	0.20%	0.08%	0.22%

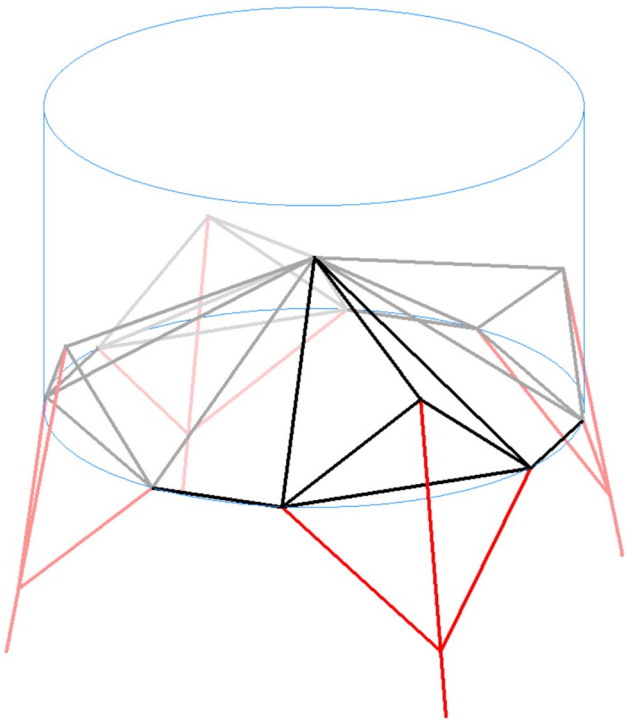

Fig. 6 Trimetric view of the truss structure of an exemplary four-legged lander

Each of these beams has a total of 12 DoF in three-dimensional space: two ends with three translational and three rotational DoF each. The local coordinate system for each of the struts has its x_1-axis in the direction of the beam. As we assume rotationally symmetric beams, the exact direction of the x_2- and x_3-axis is not important as long as they are orthogonal to the beam direction and each other. The free body forces are assumed to be positive in the axes directions. [23, 24, 28]

Once all nodes and beams are defined, the displacements and stress results at the end nodes of each beam are connected with one another [23, 24, 28]. This is done for each of the beams and is in the following explained exemplary for one beam element b connecting the nodes j and k. A depiction of this beam element is shown in Fig. 7.

The resulting forces (F) and moments (M) at the ends j and k of the beam b are combined into a stiffness relation s^b. This vector is the result of multiplying the stiffness matrix k^b of the beam with its displacement u^b (Eq. (8)):

$$s^b = \begin{pmatrix} F_1^j \\ F_2^j \\ F_3^j \\ M_1^j \\ M_2^j \\ M_3^j \\ F_1^k \\ F_2^k \\ F_3^k \\ M_1^k \\ M_2^k \\ M_3^k \end{pmatrix} = k^b \begin{pmatrix} u_1^j \\ u_2^j \\ u_3^j \\ \varphi_1^j \\ \varphi_2^j \\ \varphi_3^j \\ u_1^k \\ u_2^k \\ u_3^k \\ \varphi_1^k \\ \varphi_2^k \\ \varphi_3^k \end{pmatrix} = k^b u^b \tag{8}$$

Where

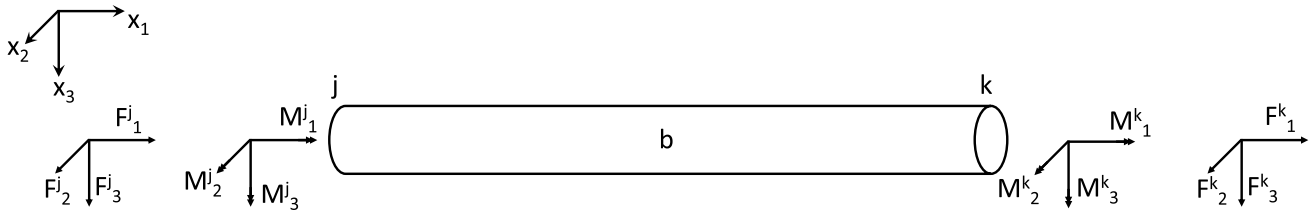

Fig. 7 Beam element with complete stress resultants in three-dimensional space (adapted from [24])

$$
\mathrm{k^b} = \begin{bmatrix}
\frac{EA}{L} & 0 & 0 & 0 & 0 & 0 & -\frac{EA}{L} & 0 & 0 & 0 & 0 & 0 \\
 & \frac{12EI_{33}}{L^3} & 0 & 0 & 0 & \frac{6EI_{33}}{L^2} & 0 & -\frac{12EI_{33}}{L^3} & 0 & 0 & 0 & \frac{6EI_{33}}{L^2} \\
 & & \frac{12EI_{22}}{L^3} & 0 & -\frac{6EI_{22}}{L^2} & 0 & 0 & 0 & -\frac{12EI_{22}}{L^3} & 0 & -\frac{6EI_{22}}{L^2} & 0 \\
 & & & \frac{GI_{11}}{L} & 0 & 0 & 0 & 0 & 0 & -\frac{GI_{11}}{L} & 0 & 0 \\
 & & & & \frac{4EI_{22}}{L} & 0 & 0 & 0 & \frac{6EI_{22}}{L^2} & 0 & \frac{2EI_{22}}{L} & 0 \\
 & & & & & \frac{4EI_{33}}{L} & 0 & -\frac{6EI_{33}}{L^2} & 0 & 0 & 0 & \frac{2EI_{33}}{L} \\
 & & & & & & \frac{EA}{L} & 0 & 0 & 0 & 0 & 0 \\
 & & & & & & & \frac{12EI_{33}}{L^3} & 0 & 0 & 0 & -\frac{6EI_{33}}{L^2} \\
 & & & & & & & & \frac{12EI_{22}}{L^3} & 0 & \frac{6EI_{22}}{L^2} & 0 \\
 & & & & & & & & & \frac{GI_{11}}{L} & 0 & 0 \\
 & & & & & & & & & & \frac{4EI_{22}}{L} & 0 \\
 & & & & & & & & & & & \frac{4EI_{33}}{L}
\end{bmatrix} \quad (9)
$$

sym.

These local vectors and matrices are transformed into a global coordinate system to calculate the stiffness matrix for the whole system. By using rotation matrices as the one in Eq. (6), the local stiffness matrices are transformed into the global coordinate system. Because the system contains a total of four three-dimensional vectors (two force vectors and two torque vectors, one for each end of the beam), a 12×12 rotation matrix C is constructed from the 3×3 rotation matrix R following the pattern shown in Eq. (10). The transformation from global to local coordinates is done by pre-multiplying the *C*-matrix with the global coordinates. Reversing this operation requires the transposed rotation matrix $\mathrm{C^T}$ [23, 24].

$$
\mathrm{C} = \begin{bmatrix} \mathrm{R} & 0 & 0 & 0 \\ 0 & \mathrm{R} & 0 & 0 \\ 0 & 0 & \mathrm{R} & 0 \\ 0 & 0 & 0 & \mathrm{R} \end{bmatrix} \quad (10)
$$

Transformation of the local stiffness matrix to the global one follows the scheme shown in Eq. (11), which is based on Eq. (8) as well as the transformation logic described in the last paragraph.

$$
\mathrm{k^b_{glob}} = \frac{\mathrm{s^b_{glob}}}{\mathrm{u^b_{glob}}} = \frac{\mathrm{C^T s^b_{lcl}}}{\mathrm{u^b_{glob}}} = \frac{\mathrm{C^T k^b_{lcl} u^b_{lcl}}}{\mathrm{u^b_{glob}}} = \frac{\mathrm{C^T k^b_{lcl} C u^b_{glob}}}{\mathrm{u^b_{glob}}} = \mathrm{C^T k^b_{lcl} C} \quad (11)
$$

Once all global stiffness relations have been computed, they are combined into an overall stiffness relation $\mathrm{S = KU}$ for the entire lander truss system as shown in Fig. 6. This is done by splitting the matrix and vectors of each strut as depicted in Eq. (12) and sorting their parts into the system stiffness relation. For each node, the degrees of freedom are defined in the U vector while the forces and torques are defined in the S vector. External forces are then inserted into the corresponding positions of the S vector. By setting the displacement of the bearing nodes in the U vector to zero, according to the boundary conditions of the system, rigid-body movement is blocked and the system is defined. If this part is neglected, the system becomes singular and therefore unsolvable [23, 24, 28].

$$
\begin{pmatrix} s^b_j \\ s^b_k \end{pmatrix} = \begin{bmatrix} k^b_{jj} & k^b_{jk} \\ k^b_{kj} & k^b_{kk} \end{bmatrix} \begin{pmatrix} u^b_j \\ u^b_k \end{pmatrix} \quad (12)
$$

Sorting the four sub-matrices of the global element stiffness matrix $\mathrm{k_{glob}}$ of each strut into K it follows that:

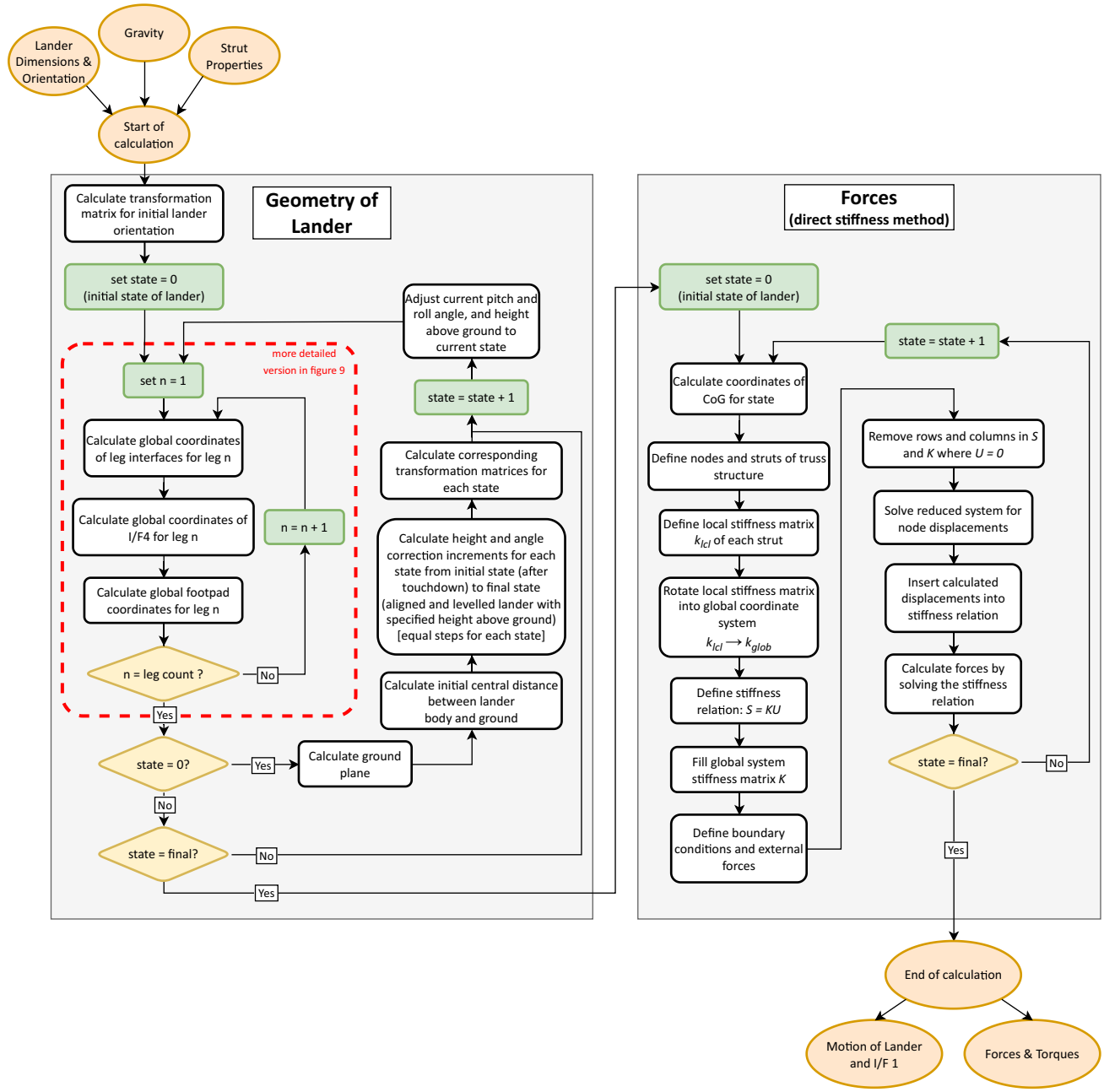

Fig. 8 Overview flowchart of the MATLAB script

$$K = \begin{bmatrix} \sum_{i=1}^{n} k_{11}^{i} & \cdots & \sum_{i=1}^{n} k_{1m}^{i} \\ \vdots & \ddots & \vdots \\ \sum_{i=1}^{n} k_{m1}^{i} & \cdots & \sum_{i=1}^{n} k_{mm}^{i} \end{bmatrix} \tag{13}$$

where n is the number of struts and m is the number of nodes.

After the external forces, boundary conditions, and stiffness matrices are sorted into their corresponding space, the equation system can be solved. It should be noted that solving the equation system is done in two steps:

1. All rows and their corresponding columns in the K matrix which contain a zero in the U vector are erased. The reduced system is then solved.

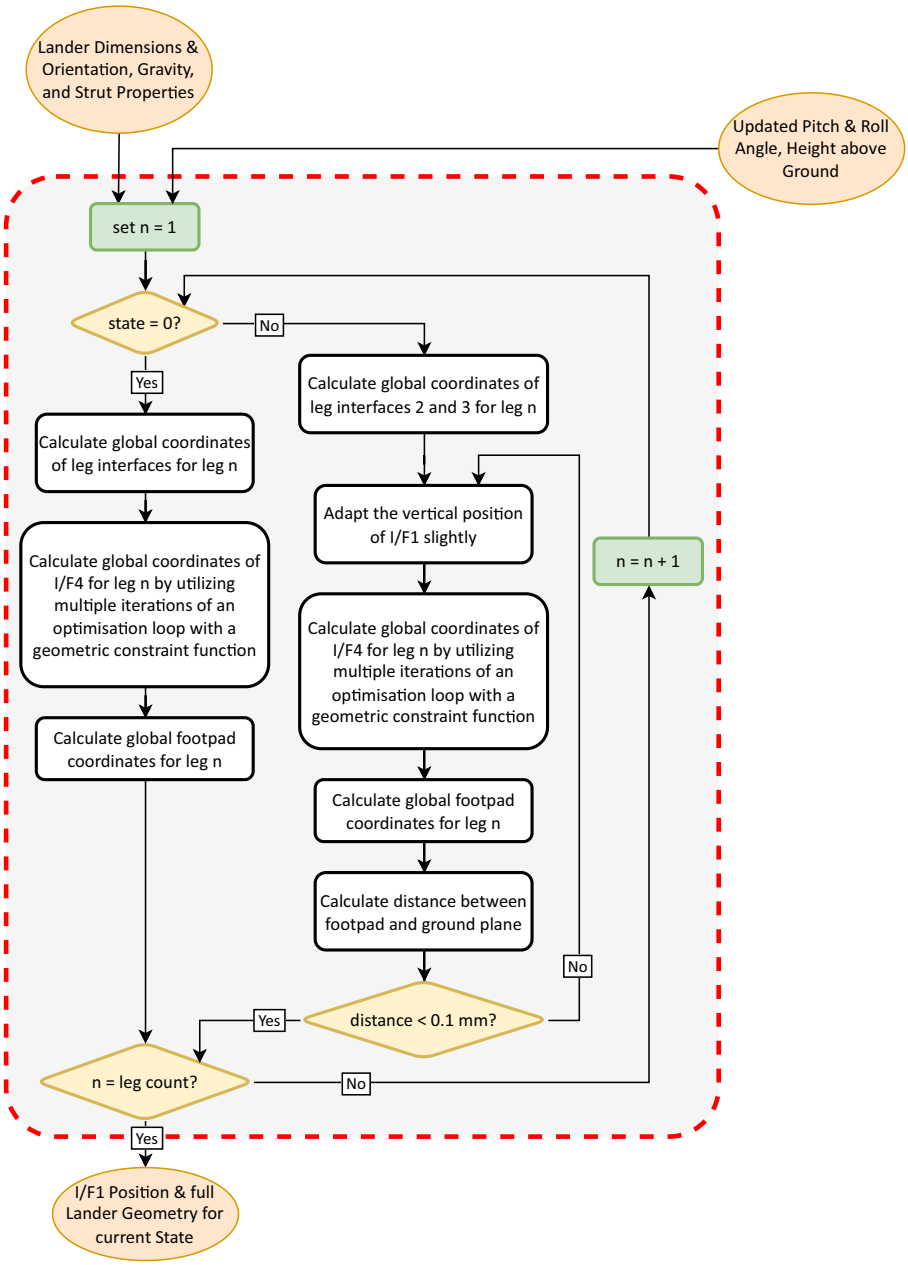

Fig. 9 More detailed flowchart of the calculation of the interface coordinates of the lander

2. The solution of the reduced system is reintroduced into the entire system, which can then be solved and yields the reaction forces of the bearing nodes as a result.

To get the forces in the beam elements, the displacements of the nodes at each end are rotated back into the local coordinate system of the respective beam element. By using Eq. (8), the forces in the element are calculated [23, 24, 28].

2.7 Numerical implementation

The numerical model to calculate the motion of the lander is implemented in MATLAB with Figs. 8 and 9 depicting the main routine. The variables defining the lander geometry (including number of legs, length of leg struts, size of lander body, and coordinates of the CoG and of the leg interfaces), mass of the lander, its initial orientation, and the mechanical properties of the struts, are imported into the script. Afterwards, the calculation commences, starting with the geometric calculation and followed by the force calculation. In the geometric calculation, the complete motion of the lander is calculated in as many discrete steps as specified. Increasing

the number of steps leads to better results in the intermediate steps between the landing state and the final state, which is great to get a more detailed understanding of the behaviour of a specific design. This does, however, come at the cost of longer calculation times. At the same time, lowering the number of calculated steps can be used to get results quickly for the comparison of different lander designs. The forces are then calculated afterwards for each step, once the geometric calculation has reached an aligned and levelled state with the specified ground distance.

2.8 Validation of force computation

The validation of the afore described DSM is done by comparing the results of an exemplary calculation achieved by the DSM in MATLAB with the results from an FEA program. For this purpose, MSC Patran 2018 and MSC Nastran with the solver SOL101, are utilised as pre-/post-processor and solver, respectively. The underlying method is nearly identical, however, this comparison still proves correct implementation and viability for future work and allows to fix possible bugs in the code.

The criteria for a successful validation were chosen as a difference of less than 1% between the results of the DSM and the FEA calculation when comparing the absolute forces acting on one leg. The orientation in question is the lander in its initial configuration, before adjusting the I/F1 positions on a 15° slope tilted only towards leg 1 (roll of 0°; pitch of 15°). This configuration puts the highest load on a single leg.

The struts are implemented as one-dimensional beam elements, allowing for bending. As only a quasi-static case is considered, the footpads are fixed in all translational directions. To make sure that the primary strut is considered as one connected beam, all rotational DoFs are fixed at I/F4. The considered lander has a mass of 5000 kg and is subjected to lunar gravitational acceleration at 1.625 m/s^2. Note that a multitude of different orientations of the lander have been compared, all of which showed similar results. The one with the largest difference between the results of DSM and FEA, that was found for a maximum tilt of 15°, is shown here.

The results of the comparison are listed in Table 1.

It is found that the largest absolute as well as relative difference between the results of the two different methods is in the direction of x_{body} on leg 3, which is the least loaded leg in this configuration. The leg experiencing the highest load in this configuration is leg 1, which is the one that has to be considered for dimensioning. Hence, the difference found in the results of leg 3 is not as critical as if it was on the leg experiencing the highest load. Additionally, the absolute force difference in leg 3 is still small compared to the absolute loads in leg 1. Finally, when calculating the absolute axial compression of the leg struts, the difference between the two methods never exceeds 4.6 N or 0.22% in this example, fulfilling the 1% maximum difference specified before. Other cases performed comparably. The DSM can therefore be used for the proposed application.

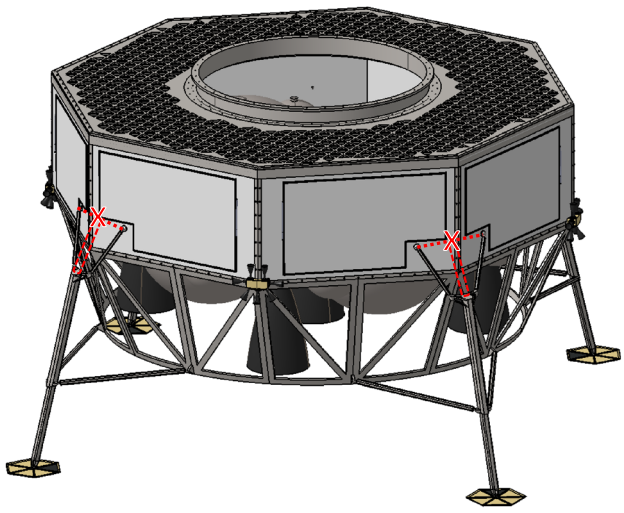

Fig. 10 CAD model of Argonaut from ESA [3]: alternative I/F1 location used for computation marked with an "x"

3 Exemplary results

The ESA published a concept of the so-called Argonaut, a lunar lander currently in development and planned to be launched in the early 2030s. A corresponding preliminary computer aided design (CAD) model, cf. Figure 10, of Argonaut from 2021 is also available for download [3].

Based on the dimensions of this CAD model and the information given in [3], a calculation using the programmed tool explained in this publication is conducted. It should be noted that the tool is conceptualised for a single I/F1 point. Hence, the two points of contact of Argonaut are replaced with a single point in the centre of the two coordinates of the CAD model. The CAD model is shown in Fig. 10 where the alternative location for I/F1 used for the computation is marked with an "x" and the leg is extended to connect to this I/F point. The exact parameters used for the calculation can be found in the appendix in Table 2.

Note that for this calculation the struts are assumed to exhibit elastic behaviour. Therefore, metallic material properties are assumed for ease of implementation. This results in a high stiffness and reduces bending of the struts. In reality, the struts are more likely to be manufactured from CFRP. CFRP, however, is not a homogenous material by design. To reduce uncertainties and inaccuracies, steel is used for this exemplary calculation. The structure of the lander body itself is also simplified according to Fig. 6, i.e.

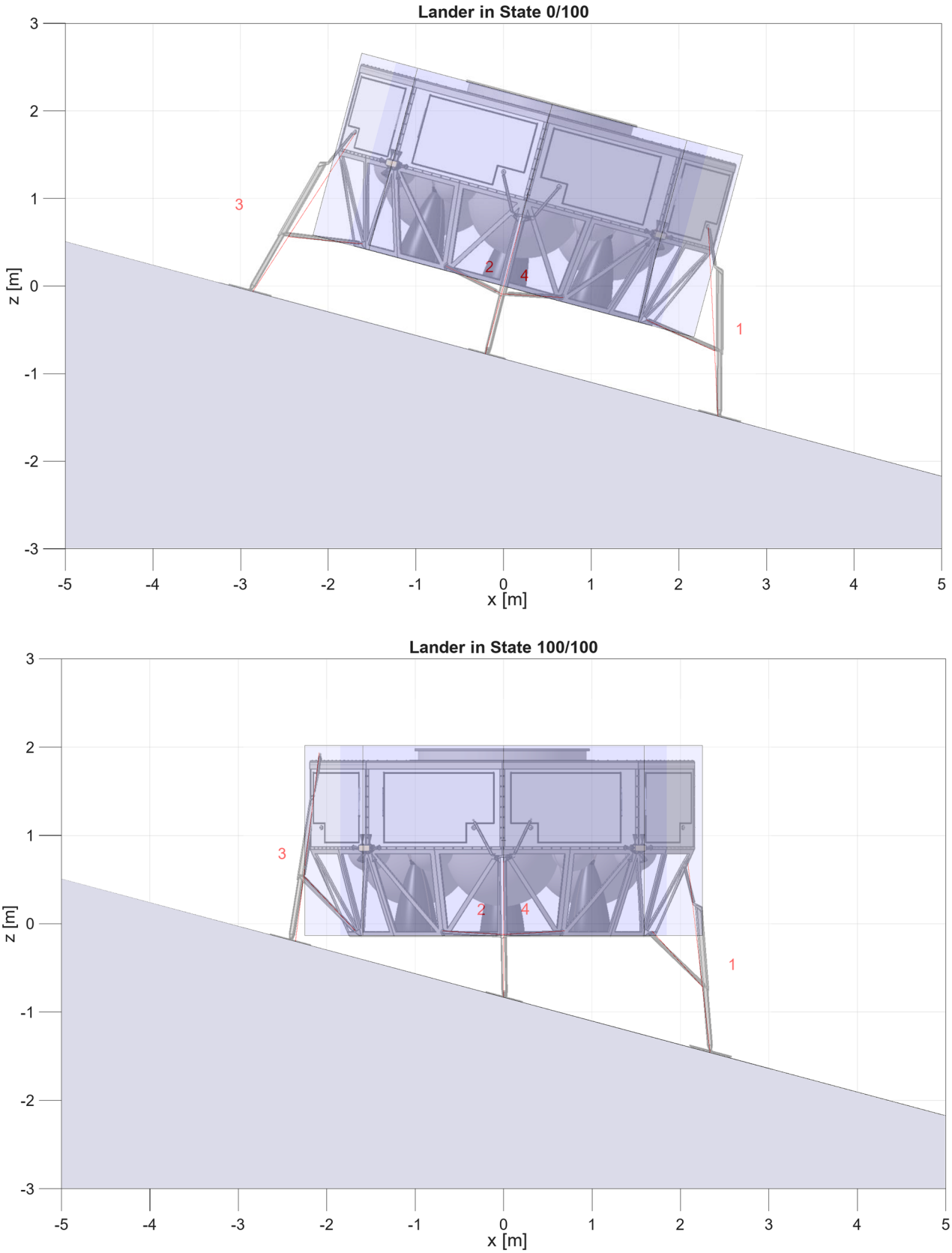

Fig. 11 Transition of Argonaut from landing position to aligned, levelled, and lowered position: State 0 and State 100 are shown here as an example of all positions calculated

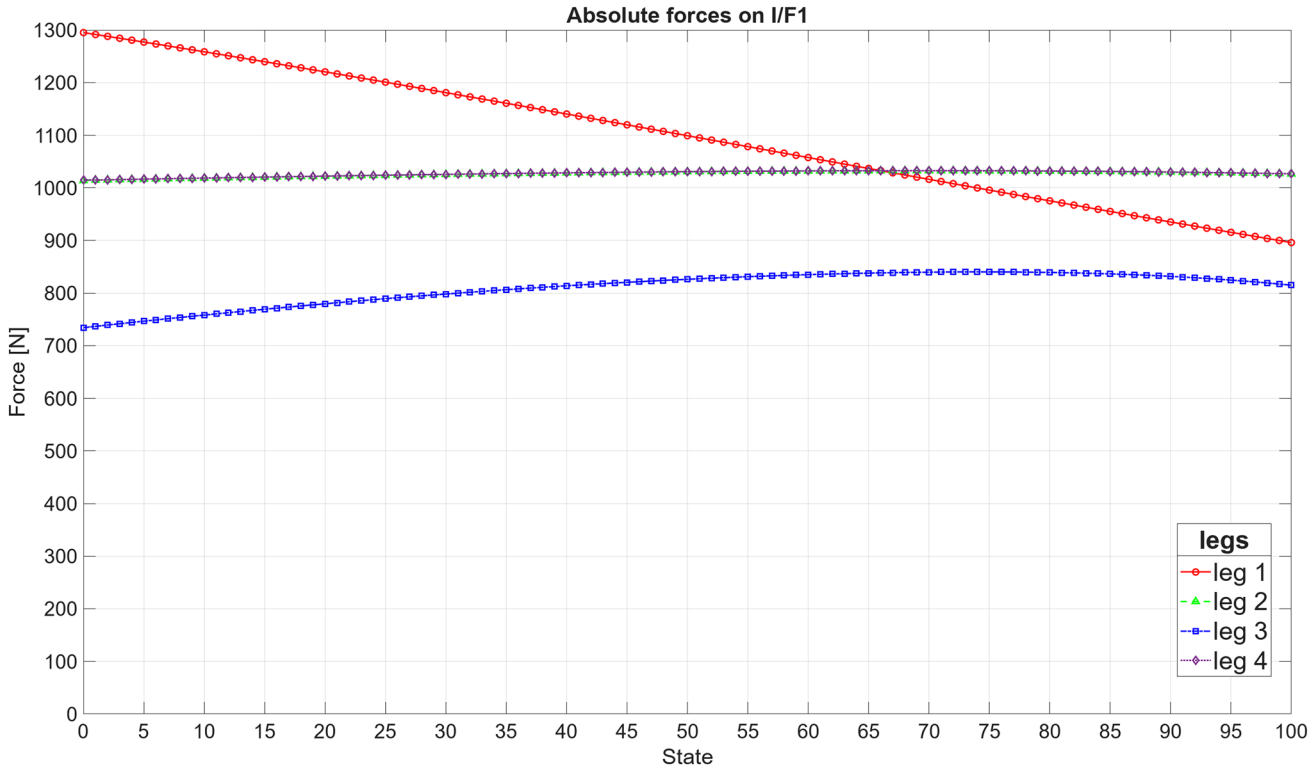

Fig. 12 Absolute forces on I/F1 for the levelling and lowering of the Argonaut lander on a 15° ground slope for each calculated State from 0 to 100

the calculation results only offer a first idea of the practicability of the design which can be used as a basis for further investigations.

Additionally, the considered tilt of the lander is in the exact direction of a single leg (as depicted in Figs. 5 and 11), i.e. the leg in the down-hill direction sees the highest load possible for the predominant ground slope, making this the worst case scenario in terms of high forces acting on a single leg. Tilting the lander in other directions shifts the load to the other legs, reducing the load on the down-hill leg.

Figure 11 shows the initial state after landing as well as the final aligned, levelled, and slightly lowered state (here State 100). The CAD model of Argonaut is shown as a transparent overlay on the calculation result from MATLAB, allowing to compare the theoretical result with the actual lander geometry. Three observations about the lander's geometry are made right here:

1. In State 100, legs 1 and 3 are almost vertical and only slightly angled outwards. This might affect the stability of the lander.
2. In State 100, I/F1 of leg 3 is located higher than the top limit of the lander body. This could lead to problems in the design of the levelling mechanism, as there might not be enough room to accommodate the mechanism, depending on its design. The same may be said about I/F1 of leg 1, which is located below the actual structure of the lander body.
3. Leg 3 intersects the lander body in the fully levelled, aligned, and lowered State 100, which would lead to problems in the real world.

All of these observations/problems could be mitigated by modifying the lengths of the leg struts or their initial interface locations, increasing the body height of the lander, limiting the acceptable ground slope angle to a lower value in which none of these problems could occur, or by a combination of these solutions.

The absolute force results for the motion of Argonaut from State 0 to State 100 can be found in Fig. 12. The first interesting result is that the maximum load on a single leg happens in State 0, i.e. the levelling and alignment operation lowers the maximum forces on the legs, while also improving the operational versatility of the lander and increasing the number of possible use cases. Due to the low gravitational acceleration on the lunar surface, the absolute force on a single leg in the quasi-static case does not exceed 1.3 kN, even though the lander has a mass of 3.7 tons. For a mechanical design, additional factors of safety have to be considered. During the transition from

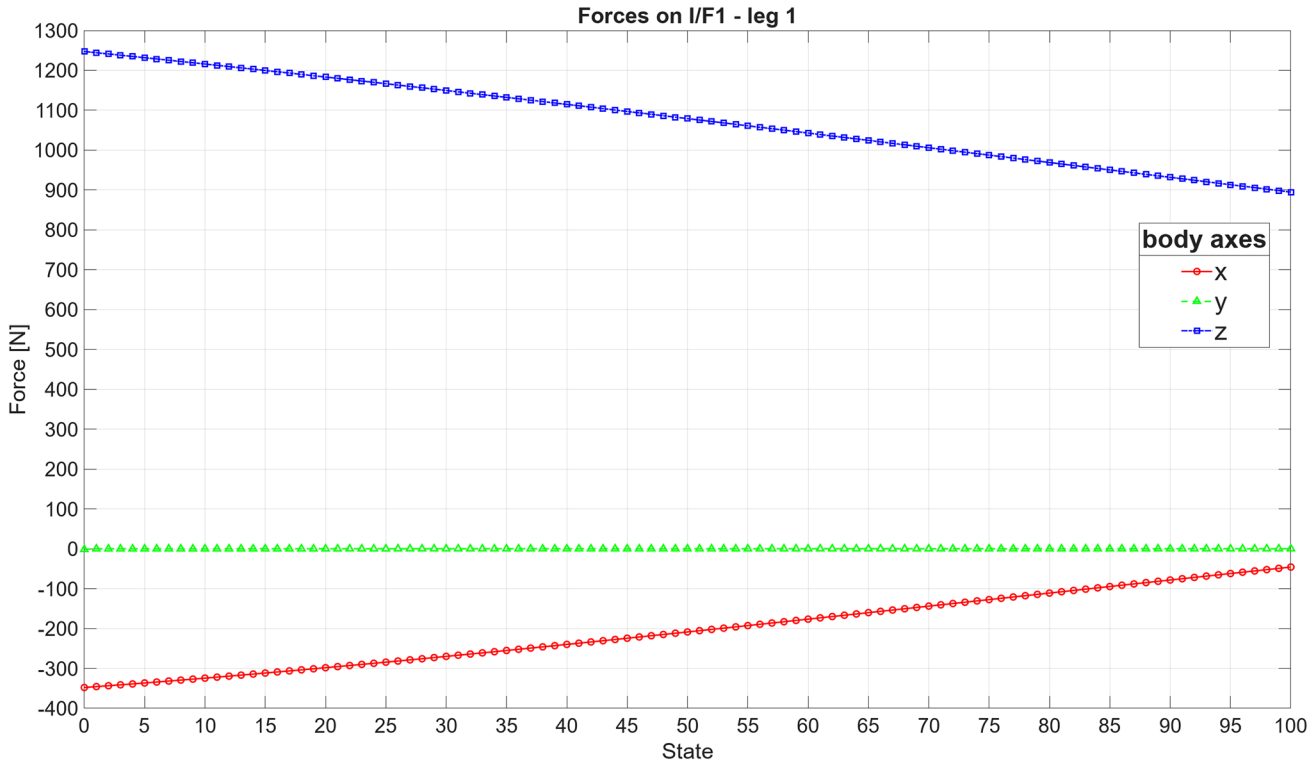

Fig. 13 Forces on I/F1 of leg 1 for the levelling and lowering of the Argonaut lander on a 15° ground slope for each calculated State from 0 to 100

State 0 to State 100, the force is slowly shifted from leg 1 to the other legs (especially leg 3 on the opposite side of the lander). Legs 2 and 4, which are located on opposite sides of the lander body but on the same height, show equal forces, as expected. Hence, the curves of leg 2 and leg 4 overlap.

Figure 13 depicts the forces in each of the three spatial directions (cf. Figure 4 for coordinate system) exemplary for leg 1, which experiences the highest load. Both the absolute force in the x_{body}- and z_{body}-direction decrease from State 0 to State 100. One reason for this effect is the shift of the load from leg 1 to the other legs, the other is the change of the angles of the struts changing the combined load on all legs.

For this example, the movement of I/F1 lies in the range of − 0.43 m and + 0.82 m in the direction of z_{body}, i.e. the length of the linear drive, moving the I/F should be at least 1.25 m to be able to level the lander on a 15° ground slope.

All of these results form a first image of whether a design might work or where its limits lie, allowing to quickly make design changes in early project stages. Additionally, the fact that many possible problems are revealed using a singular calculation highlights the power that the calculation explained in this publication offers.

4 Discussion and concluding remarks

Including an alignment and levelling kinematic on exploration landing platforms is no trivial task. Many effects have to be considered when designing and operating such a kinematic. From the general movement of the landing leg struts, over the uneven terrain on the lunar (or other celestial body) surface, to coupling effects due to the way a parallel kinematic functions, many challenges have to be overcome. Being able to quickly discern whether a design is implementable and where its limits are is a valuable asset to have.

The approach explained in this publication can help to get early and fast results as a basis for further examination of a specific design. It has some limits regarding the representation of all effects present during an alignment, levelling, and lowering operation. In future applications, it shall be expanded in regards to different surface conditions, unevenness in the ground slope, friction, parasitic motion, dynamic effects (that are not completely negligible even for slow movement), or the shift of the CoG that occurs when the leg configuration is changed or the contents of the fuel tanks shift while tilting the lander.

In the current state, this quick approach to calculating lander motion presented here, enables the examination of motion throughout different discrete steps along the alignment,

levelling, and lowering process using the provided graphs (e.g. see Figs. 5 or 11). Using this data, it is possible to find limiting factors for a specific lander design such as the maximum possible ground angle that can be dealt with before reaching an unstable state. By changing the lander's modelling parameters, quick changes to strut lengths or interface positions can be made to improve the overall design and capability of the lander early on. Extrema of the to-be-expected forces and the behaviour of these forces on each of the legs and interfaces during the levelling operation can be examined. The approach was validated using MSC Nastran (SOL101), i.e. the results can be used for a first sizing of a levelling and lowering kinematic prior to complex analysis using an FEA program.

In conclusion, the method described in this publication offers the possibility to investigate a multitude of different lander configurations (including cantilever and inverted tripod) for the implementation of an alignment, levelling, and lowering kinematic. It only uses basic parameters of early design stages of the lander design and only includes intrinsic properties that are measured automatically from within the lander itself. It can be automated for the comparison of small design variations. This approach can help to improve the design in early project stages and to increase the operational limits of the lander in regards to stability and operational versatility.

Appendix

See Table 2.

Table 2 Parameters used for exemplary Argonaut calculation

Symbol	Parameter	Value		
Coordinates				
Type of coordinate		*x*	*y*	*z*
Coordinate of I/F1 (exemplary for leg 1)*[1]		2084 mm	0 mm	1250 mm
Coordinate of I/F2 (exemplary for leg 1)*[1]		1676 mm	− 694 mm	50 mm
Coordinate of I/F3 (exemplary for leg 1)*[1]		1676 mm	694 mm	50 mm
Coordinate of CoG*[1]		0 mm	0 mm	1075 mm
Dimensions				
d_L	Diameter of lander body	4500 mm		
$h_{L,pre}$	Height of lander body	2150 mm		
L_{S1}	Length of primary struts	2160 mm		
$L_{S1,upp}$	Distance I/F1 to I/F4	1410 mm		
$L_{S1,low}$	Distance I/F4 to footpad	750 mm		
L_{S2}/L_{S3}	Length of secondary struts	1100 mm		
h_{CoG}	Height of CoG in lander body *[1]	1075 mm		
Masses				
m_{struct}	Mass of lander structure	1600 kg		
$m_{P/L}$	Mass of payload	2100 kg		
m_{tot}	Combined total mass of lander	3700 kg		
Ground slope/tilt of lander				
α_{gnd}	Ground slope angle	15°		
θ	Pitch of lander body	15°		
φ	Roll of lander body	0°		
Other parameters				
g_{lunar}	Acceleration due to gravity on the lunar surface	1.625 m/s^2		
$h_{gnd,post}$	Height of lander body above ground (post alignment and lowering)	100 mm		
n_{steps}	Calculation steps between initial and final position	100		
Properties of struts				
E	Young's modulus	210 GPa		
ν	Poisson's ratio	0.3		
R_{strut}	Radius of struts	150 mm		
t_{strut}	Wall thickness of struts	50 mm		

*[1]Rotational and vertical symmetry of lander body are assumed

Author contributions J.B. prepared the manuscript text and all figures. L.W. reviewed the manuscript and supervised the work. All authors have read and agreed to the published version of the manuscript.

Funding Open Access funding enabled and organized by Projekt DEAL.

Data availability No datasets were generated or analysed during the current study.

Declarations

Conflict of interest The authors declare no competing interests.

References

1. Williams, C.E.: Artemis, NASA, Apr. 24, 2024. [Online] Available: https://www.nasa.gov/artemisprogram Accessed 03 June 2024
2. Human spaceflight and robotic exploration programmes, ESA Website. [Online] Available: https://www.esa.int/About_Us/Ministerial_Council_2016/Human_Spaceflight_and_Robotic_Exploration_Programmes Accessed 03 June 2024
3. Argonaut, ESA Website. [Online] Available: https://www.esa.int/Science_Exploration/Human_and_Robotic_Exploration/Exploration/Argonaut Accessed 03 June 2024
4. Terrae Novae: Europe's exploration vision, ESA Website. [Online] Available: https://www.esa.int/Science_Exploration/Human_and_Robotic_Exploration/Exploration/Terrae_Novae_Europe_s_exploration_vision Accessed 09 Sep 2024
5. Vision and Voyages for Planetary Science in the Decade 2013–2022. National Research Council, (2011). https://doi.org/10.17226/13117
6. Bai, C., Guo, J., Zheng, H.: Optimal guidance for planetary landing in hazardous terrains. IEEE Trans. Aerosp. Electron. Syst. **56**(4), 2896–2909 (2020). https://doi.org/10.1109/taes.2019.2955785
7. Kim, Y.-B., Jeong, H.-J., Park, S.-M., Lim, J.H., Lee, H.-H.: Prediction and validation of landing stability of a lunar lander by a classification map based on touchdown landing dynamics' simulation considering soft ground. Aerospace **8**(12), 380 (2021). https://doi.org/10.3390/aerospace8120380
8. Maeda, T., Kajiwara, R., Otsuki, M., Hashimoto, T.: Proposal of an actively controllable landing leg for lunar-planetary lander. 2013 6th International Conference on Recent Advances in Space Technologies (RAST). IEEE, (2013) https://doi.org/10.1109/rast.2013.6581354
9. Shigeto, S., Fujimoto, H., Hori, Y., Otsuki, M., Hashimoto, T.: Fundamental research on reduction of impact forces using actively controlled landing gear in lunar/planetary landers. IEEJ Trans. Ind. Appl. **133**(3), 335–341 (2013). https://doi.org/10.1541/ieejias.133.335
10. Maeda, T., Ozaki, T., Hara, S., Matsui, S.: Touchdown dynamics of planetary lander with translation-rotation motion conversion mechanism. J. Spacecr. Rockets **54**(4), 973–980 (2017). https://doi.org/10.2514/1.a33630
11. Huang, M.: Analysis of rocket modelling accuracy and capsule landing safety. Int. J. Aeronaut. Space Sci. **23**(2), 392–405 (2022). https://doi.org/10.1007/s42405-021-00439-y
12. Huang, M., Nie, H., Zhang, M., Wei, X., Yue, S.: Design of mission adaptive landing gear for near space travel lander. J. Vibroeng. **18**(8), 4949–4963 (2016). https://doi.org/10.21595/jve.2016.17078
13. Manca, R., Puliti, M., Circosta, S., Galluzzi, R., Salvatore, S., Amati, N.: Design and optimization of an active leveling system actuator for lunar lander application. Actuators **11**(9), 263 (2022). https://doi.org/10.3390/act11090263
14. NASA, "AS12-46-6783", Apollo 12 Image Library. [Online] Available:https://www.nasa.gov/history/alsj/a12/images12.html#6783
15. Witte, L., et al.: A robotically deployable lunar surface science station and its validation in a Moon-analogue environment. Planet. Space Sci. **193**, 105080 (2020). https://doi.org/10.1016/j.pss.2020.105080
16. NASA Mission Evaluation Team. Apollo 15 Mission Report, National Aeronautics and Space Administration Manned Spacecraft Center, Houston, Texas, United States of America, MSC-05161, Dec. 1971. [Online] Available: https://sma.nasa.gov/SignificantIncidents/assets/apollo-15-mission-report.pdf Accessed 09 Sep 2024
17. Cheatham, D.C., Bennett, F.V., Apollo Lunar Module Landing Strategy.: Manned Spacecraft Center, Houston, Texas, United States of America: NASA, 1966. [Symposium Proceedings]. Available: http://images.spaceref.com/Apollo/ALLMS/ApolloLunar_Landing_Symposium_Proceedings.pdf Accessed 19 Feb 2025
18. Baker, D.: The history of manned space flight, 1st edn. Crown Publishers Inc., New York (1982)
19. Mareczek, J.: Inverse Kinematik. In: Grundlagen der Roboter-Manipulatoren –, vol. 1, pp. 117–145. Springer Berlin Heidelberg, Cham (2020). https://doi.org/10.1007/978-3-662-52759-7_3
20. Park, F.C.: Parallel Robots. In: Encyclopedia of systems and control, pp. 1661–1666. Springer International Publishing, Cham (2021). https://doi.org/10.1007/978-3-030-44184-5_174
21. Nigatu, H., Choi, Y.H., Kim, D.: Analysis of parasitic motion with the constraint embedded Jacobian for a 3-PRS parallel manipulator. Mech. Mach. Theory **164**, 104409 (2021). https://doi.org/10.1016/j.mechmachtheory.2021.104409
22. Lin, R., Guo, W., Gao, F.: On parasitic motion of parallel mechanisms, volume 5B: 40th mechanisms and robotics conference. Am. Soc. Mech. Eng. (2016). https://doi.org/10.1115/detc2016-59859
23. Krätzig, W.B., Harte, R., Könke, C., Petryna, Y.S.: Tragwerke 2. Springer, Berlin Heidelberg (2019). https://doi.org/10.1007/978-3-642-41723-8
24. Krämer, C.: Gewichtsvergleich verschiedener Bauweisen einer Mondstation auf Basis des Strukturkennwerts. M.Sc. thesis, Institute of Structural Mechanics and Lightweight Design, RWTH Aachen (2021)
25. Patnaik, S.: An integrated force method for discrete analysis. Int. J. Numer. Methods Eng. **6**(2), 237–251 (1973). https://doi.org/10.1002/nme.1620060209
26. Witte, L.: Touchdown dynamics and the probability of terrain related failure of planetary landing systems: a contribution to the landing safety assessment process. Ph.D. dissertation, Faculty of Production Engineering, University of Bremen, Nov. 20, 2015. [Online] Available: Media SuUB Bremen, http://nbn-resolving.de/urn:nbn:de:gbv:46-00104952-14. Accessed 05 June 2024
27. Rogers, W.F.: Apollo experience report: lunar module landing gear subsystem. NASA Lyndon B. Johnson Space Center Houston, TX,

United States, NASA Technical Note, NASA-TN-D-6850, MSC-S-316, Jun. 1, 1972. [Online] Available: NTRS – NASA Technical Reports Sever, https://ntrs.nasa.gov/citations/19720018253. Accessed 05 June 2024

28. Turner, M.J., Clough, R.W., Martin, H.C., Topp, L.J.: Stiffness and deflection analysis of complex structures. J. Aeronaut. Sci. **23**(9), 805–823 (1956). https://doi.org/10.2514/8.3664